

# Self-Referenced Method for Estimating Refractive Index and Absolute Absorption of Loose Semiconductor Powders

Huafeng Huang,<sup>†</sup> Diane M. Colabello,<sup>†</sup> Elizabeth C. Sklute,<sup>§</sup> Timothy D. Glotch,<sup>§</sup> and Peter G. Khalifah<sup>\*,†,‡,§</sup>

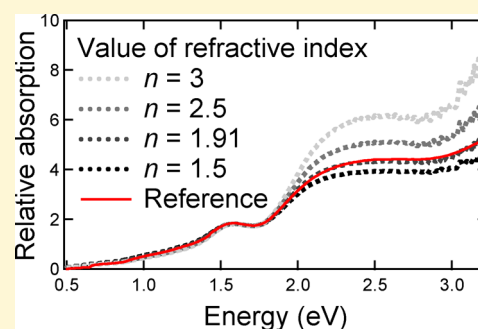
<sup>†</sup>Department of Chemistry, State University of New York at Stony Brook, Stony Brook, New York 11794-3400, United States

<sup>‡</sup>Department of Chemistry, Brookhaven National Laboratory, Upton, New York 11973, United States

<sup>§</sup>Department of Geosciences, Stony Brook University, Stony Brook, New York 11794, United States

## Supporting Information

**ABSTRACT:** The absolute absorption coefficient,  $\alpha(E)$ , is a critical design parameter for devices using semiconductors for light harvesting associated with renewable energy production, both for classic technologies such as photovoltaics and for emerging technologies such as direct solar fuel production. While  $\alpha(E)$  is well-known for many classic simple semiconductors used in photovoltaic applications, the absolute values of  $\alpha(E)$  are typically unknown for the complex semiconductors being explored for solar fuel production due to the absence of single crystals or crystalline epitaxial films that are needed for conventional methods of determining  $\alpha(E)$ . In this work, a simple self-referenced method for estimating both the refractive indices,  $n(E)$ , and absolute absorption coefficients,  $\alpha(E)$ , for loose powder samples using diffuse reflectance data is demonstrated. In this method, the sample refractive index can be deduced by refining  $n$  to maximize the agreement between the relative absorption spectrum calculated from bidirectional reflectance data (calculated through a Hapke transform which depends on  $n$ ) and integrating sphere diffuse reflectance data (calculated through a Kubelka–Munk transform which does not depend on  $n$ ). This new method can be quickly used to screen the suitability of emerging semiconductor systems for light-harvesting applications. The effectiveness of this approach is tested using the simple classic semiconductors Ge and  $\text{Fe}_2\text{O}_3$  as well as the complex semiconductors  $\text{La}_2\text{MoO}_5$  and  $\text{La}_4\text{Mo}_2\text{O}_{11}$ . The method is shown to work well for powders with a narrow size distribution (exemplified by  $\text{Fe}_2\text{O}_3$ ) and to be ineffective for semiconductors with a broad size distribution (exemplified by Ge). As such, it provides a means for rapidly estimating the absolute optical properties of complex solids which are only available as loose powders.



## INTRODUCTION

The absorption coefficient of semiconductor,  $\alpha(E)$ , determines what thickness of a material is required to effectively absorb light of a particular wavelength. As such, the absolute absorption coefficient is a critical design parameter for semiconductors used for light-harvesting applications associated with renewable energy production. The applications include the mature technology of electricity generation by photovoltaic devices as well as alternative technologies for the production of chemical fuels through water oxidation or  $\text{CO}_2$  reduction. The absorption behavior clearly impacts the material cost of the semiconductor device (which is expected to scale with thickness) but may have an even larger impact on functionality since the length that photogenerated free carriers can diffuse before recombining is often small relative to the semiconductor thickness needed to harvest the majority of light illuminating the semiconductor. While  $\alpha(E)$  is well-known for many classic semiconductors used in photovoltaic applications, the absolute values of  $\alpha(E)$  are typically unknown for the complex semiconductors being explored for emerging applications such as the solar production of  $\text{H}_2$  fuel from water,<sup>1–4</sup> the reduction of  $\text{CO}_2$  to form

hydrocarbon fuels,<sup>5</sup> or unconventional ferroelectric photovoltaics.<sup>6</sup>

The fundamental equation describing the absorption of light of a given wavelength is  $I/I_0 = e^{-\alpha t}$ , where the ratio of the intensity of the transmitted ( $I$ ) and incident ( $I_0$ ) light scales as the negative exponent of the product of the absorption coefficient ( $\alpha$ ) and the material thickness ( $t$ ). In order to absorb  $\sim 90\%$  of incident light, the material thickness must be at least  $t = 2/\alpha$ . For a strongly absorbing optical transition with  $\alpha \sim 10^5 \text{ cm}^{-1}$  this corresponds to a thickness of  $\sim 200 \text{ nm}$ , while for a weakly absorbing transition with  $\alpha \sim 10^2 \text{ cm}^{-1}$  this corresponds to a much larger thickness of  $\sim 200 \mu\text{m}$ , which is far larger than the free carrier diffusion length expected for semiconductors. In many cases, it has been found that the measured photoactivity of semiconductor systems scales linearly with the absorption coefficient (Figure 1), indicating that the absorption behavior of the semiconductor is critically limiting performance.<sup>3,7</sup> This is

Received: October 19, 2016

Revised: April 23, 2017

Published: April 23, 2017

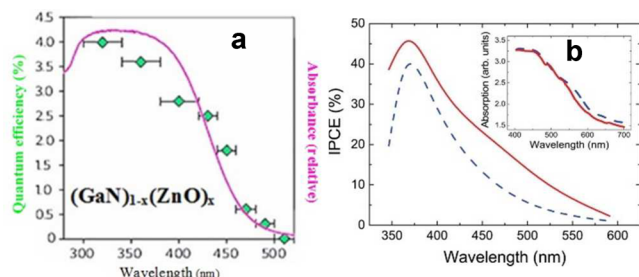


**Figure 1.** Two photoactive semiconductor systems in which the quantum efficiency scales with absorption. (a) Overall water splitting by a  $(\text{GaN})_{1-x}(\text{ZnO})_x$  semiconductor. [Reference 3. Reprinted by permission from Macmillan Publishers Ltd., copyright 2006.] (b) Water oxidation by hematite  $\text{Fe}_2\text{O}_3$ . [Reprinted with permission from ref 7. Copyright 2011 The Electrochemical Society.]

not surprising since the absorption coefficient often has a strong wavelength dependence and may vary by multiple orders of magnitude across the photon energies most relevant for solar applications (1–4 eV).

While the determination of the *relative* absorption spectrum, here denoted  $\alpha'(E)$ , of semiconductor can be easily accomplished using commercial instruments that utilize an integrating sphere to measure the diffuse reflectance of powders, the measurement of *absolute* absorbance coefficients, denoted  $\alpha(E)$ , is far from routine. For this reason, the absolute absorbance coefficients for the vast majority of emerging complex semiconductor systems remain unknown. If large, highly perfect single crystals or crystalline epitaxial films are available,  $\alpha(E)$  can be determined in a relatively straightforward manner based on measurements of the transmission or reflectance spectrum.<sup>8,9</sup> However, it can be the work of many months or years to prepare samples suitable for these measurements. Alternatively, dense pellets of polycrystalline powders can be used to determine  $\alpha(E)$  through the application of a Kramers–Kronig transform to reflectance data collected over a very wide range of energies (approximately 0.001–10 eV). Still, there are significant hurdles in both sample preparation (should have very dense pellets polished to have a high reflectivity), instrumentation (coverage of this energy range typically requires the use of many different sources and detectors, and the absolute reflectance must be determined so standard reference materials need to be used to calibrate the data seamlessly across all of the separate measurements), and in the method itself (knowledge about the reflectance at all frequencies is needed for the Kramers–Kronig transform, so approximations must be made about the sample response outside the measurement range).<sup>10</sup> As a result, this very laborious method still has substantial accuracy limitations.<sup>11</sup>

In this work, a simple self-referenced method compatible with loose powder samples is demonstrated, allowing the estimation of both refractive indices,  $n(E)$ , and absolute absorption coefficients from diffuse reflectance data. This method can be quickly used to screen the suitability of emerging semiconductor systems for light-harvesting applications, even if the semiconductors are only available as loose powders, maximizing its versatility and applicability. In this approach, diffuse reflectance data are first collected using an integrating sphere and transformed to a  $\alpha'(E)$  through a Kubelka–Munk transform. Next, bidirectional reflectance data are collected for the same powder. A mathematical transform for calculating  $\alpha(E)$  from bidirectional reflectance data has been derived previously by Hapke,<sup>12–14</sup> and this approach requires knowledge of both  $n(E)$

and particle diameter,  $D$ . There are a variety of well-known experimental methods for measuring  $D$ . Here, it is experimentally demonstrated that the refractive index can be determined in a self-referenced manner by comparing the relative absorption obtained using both integrating sphere and bidirectional reflectance methods. When these two inputs are combined, reasonable estimates of  $\alpha(E)$  values of complex semiconductors can be made. It is shown that this new approach works well for semiconductors with narrow size distributions and a broad (in energy) response, as seen for a sample of  $\text{Fe}_2\text{O}_3$ . In contrast, it is found that wide particle size distributions and a narrow absorption lead to poor estimates, as seen for a sample of Ge.

## ■ EXPERIMENTAL SECTION

Powders of hematite  $\text{Fe}_2\text{O}_3$  (99.945%, Alfa Aesar) and Ge (99.999%, STREM Chemicals, Inc.) were obtained from commercial suppliers. These powders were hand ground in an agate mortar and pestle prior to reflectance measurements. The ternary compounds  $\text{La}_2\text{MoO}_5$  and  $\text{La}_4\text{Mo}_2\text{O}_{11}$  were prepared from starting materials of  $\text{La}_2\text{O}_3$  (99.99%, Alfa Aesar) and  $\text{MoO}_3$  (99.95%, Alfa Aesar).  $\text{La}_2\text{O}_3$  was dried at 900 °C for several hours before weighing. For both compounds, stoichiometric amounts of the starting materials were ground using an agate mortar and pestle and then placed in a dense alumina crucible (CoorsTek). For the synthesis of both  $\text{La}_2\text{MoO}_5$  and  $\text{La}_4\text{Mo}_2\text{O}_{11}$  the precursors were reacted in air in a box furnace at 950 °C for about 12 h to form an intermediate phase of  $\text{La}_2\text{MoO}_6$ .  $\text{La}_2\text{MoO}_5$  was then obtained by heating a 1/2 in. diameter pellet of  $\text{La}_2\text{MoO}_6$  in a 1 in. i.d. quartz tube under a flowing gas mixture of 5/95  $\text{H}_2/\text{N}_2$  (60 mL/min, passed through a line drier) in a Lindberg/BlueM Mini-Mite furnace at temperatures of 900–950 °C for about 3 days with intermediate grinding. Upon completion of the reaction, the powder was slate gray in color.  $\text{La}_4\text{Mo}_2\text{O}_{11}$  (~10 g) was synthesized by heating  $\text{La}_2\text{MoO}_6$  at 900 °C in a reducing atmosphere of 5/95  $\text{H}_2/\text{N}_2$  (60 mL/min) in a Mellen SV Series mullite tube (3.5 in. diameter) furnace for about 10 days with intermediate grindings. The final product was dark gray in color. Reaction progress was assessed using laboratory powder X-ray diffraction data (XRD) collected over a  $2\theta$  scan range of 10–119° using a step size of 0.02°, a fixed divergence slit of 0.3°, and Soller slit widths of 2.5° on a Bruker D8 Advance diffractometer with a nickel filtered  $\text{Cu K}\alpha$  source.

Scanning electron microscopy (SEM) data were collected on a JEOL 7600F instrument. Powder samples were mounted on circular aluminum standard sample studs using carbon conductive tape. To minimize sample overlap, samples were dispersed in ethyl alcohol prior to deposition on carbon tape. The ImageJ analysis software<sup>15</sup> was used for estimating particle size distributions. Laser diffraction on a Malvern Mastersizer 2000 diffractometer was used as complementary technique for the determination of particle size. For these experiments, solutions were mixed overnight to disperse and homogenize them prior to measurements. During measurements, a small portion of the suspended powders was pipetted into a 600 mL beaker by a Hydro 2000MU pump and the sample was further diluted and sonicated to reach an optimal transmission through the sample cell. For each sample, the tested dispersant solutions were water, ethyl alcohol, water with surfactant, and water with sodium hexametaphosphate. Final measurements were carried out using sodium hexametaphosphate, which was found to be the optimal dispersant.

High energy optical data were collected in UV–vis diffuse reflectance spectroscopy on a PerkinElmer Lambda 950

spectrometer coupled with a 60 mm integrating sphere. Powder samples were loaded into a cylindrical powder holder with a circular quartz window 16.60 mm in diameter and 1.50 mm thick. A scan range of 250–860 nm (4.97–1.44 eV) with a lamp change at 319.2 nm was used with a step size of 1.30 nm and a scan rate of 182.25 nm/min. Calibration was done using a BaSO<sub>4</sub> (Alfa Aesar, 99.998%) 100% reflectance standard. Integrating sphere reflectance data,  $R(E)$ , were transformed to a relative absorption,  $\alpha'_{IS}(E)$ , by a Kubelka–Munk transform.<sup>16</sup>

Low energy optical data were collected on a bidirectional reflectance spectrometer (Supporting Information Figure S5) using an 8° field of view (optic lens coupled to the detector through an optical fiber) on an ASD Fieldspec3Max UV–vis–near-IR spectrometer with a 512 element Si photodiode array detector for the 350–1000 nm energy range and two thermoelectric-cooled InGaAs photodiode detectors in the 1000–2500 nm range, giving a spectral resolution of 10 nm (at 1400 and 2100 nm). The incident light was provided by an Ocean Optics HL-2000-HP tungsten halogen light source directed down a 600 mm Ocean Optics optical fiber. Data were collected with an incidence angle  $\theta_i$  of 30° and an emission angle  $\theta_e$  of 0° (angles specified relative to normal of the sample plane). Incidence and emergence angles were set using a custom-built mount (estimated error < 2°). All spectra were taken in the absence of ambient light and referenced to a calibrated Spectralon standard (Labsphere, Inc.) illuminated at the same angle as the sample. Reflectance data were taken at 10 scans/s by averaging 500 dark current scans, 500 white reflectance reference scans, and 500 sample reflectance scans. Powder samples were loaded into a black sample holder with a well depth of 5 mm and then leveled by tapping of the sample holder.

## RESULTS AND DISCUSSION

**Hapke Theory for Bidirectional Reflectance Data.** A general treatment of the scattering of light from powder samples has been derived by Hapke<sup>14</sup> (Figure S1). The geometry for a bidirectional reflectance experiment is shown in Figure 2. In the

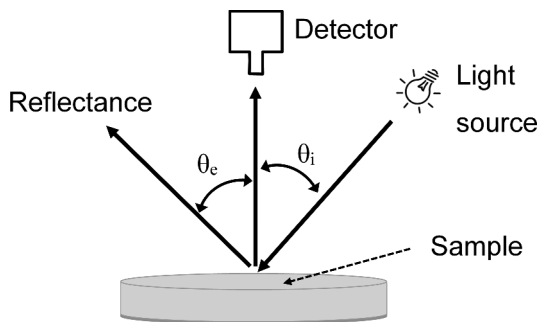


Figure 2. Bidirectional reflectance data collection geometry.

present work, the incidence angle,  $\theta_i$ , was set to 30° while the emission angle,  $\theta_e$ , was set to 0°, putting the detector normal to the flat sample tray containing the loose powder. The specific relationship expected between the experimentally measured bidirectional reflectance response and the sample absolute absorbance under a simple set of approximations within that general formalism of Hapke is reviewed here.

The first step to determining  $\alpha(E)$  is the calculation of the single-scattering albedo,  $w$ . This is defined as the ratio of scattering to total extinction (scattering + absorption).  $w$  is related to the albedo factor,  $\gamma$ , by

$$w = 1 - \gamma^2 \quad (1)$$

$\gamma$  at a specific wavelength can be derived from the measured reflectance,  $R$ , by

$$\gamma = \frac{\sqrt{(\mu_0 + \mu)^2 R^2 + (1 + 4\mu_0\mu R)(1 - R)} - (\mu_0 + \mu)R}{1 + 4\mu_0\mu R} \quad (2)$$

where  $\mu_0$  and  $\mu$  are the cosine of  $\theta_i$  and  $\theta_e$ , respectively. The internal transmission coefficient,  $\Theta$ , describes the total fraction of light entering the particle that reaches its surface after one transit, and it depends on the single-scattering albedo as

$$\Theta = \frac{w - S_e}{1 - S_e - S_i + S_i w} \quad (3)$$

Here,  $S_e$  and  $S_i$  are the external and internal scattering coefficients. For nonporous materials, it has been proposed<sup>13,14</sup> that these scattering coefficients can be approximated by

$$S_i \approx 1.014 - \frac{4}{n(n+1)^2} \quad (4)$$

$$S_e \approx \frac{(n-1)^2 + k^2}{(n+1)^2 + k^2} + 0.05 \quad (5)$$

where  $n$  is the real part and  $k$  is the imaginary part of the refractive index. Both equations are empirical formulations approximated from exact values of  $S_e$  and  $S_i$ . For a specific wavelength, the absorption depends on  $k$  as

$$\alpha = \frac{4\pi k}{\lambda} \quad (6)$$

For nonmetallic samples, the interaction of light with the solid is typically weak. As a result of this, it is usually true that  $k < 0.1$ , and as a consequence, the influence of  $k$  on  $S_e$  is small. For example, at a wavelength of 600 nm—near the center of the visible light spectrum—the value of  $k$  will be less than 0.1 so long as the absorption coefficient is below  $\sim 2 \times 10^4 \text{ cm}^{-1}$ . The reflectance data will therefore generally provide good sensitivity to the refractive index,  $n(E)$ . Conversely, the same arguments suggest that sensitivity of the method to very strong absorption features may be limited. It should be noted that in the presence of very strong absorption ( $k > 0.1$ ), the simple expressions for  $S_i$  and  $S_e$  in eqs 4 and 5 in which  $n$  and  $k$  independently contribute to the scattering coefficients may not be appropriate.<sup>14</sup>

In general,  $\Theta$  can also independently be related to the absorption coefficient,  $\alpha$ , and the distance light travels through particles by the relationship:

$$\Theta = e^{-\alpha \langle D \rangle} \quad (7)$$

Note that  $\langle D \rangle$  is the effective particle thickness and is defined as the distance traveled by rays that traverse the particle once without being internally scattered, and for ideal monodisperse spheres, this effective distance is about 90% of the diameter, with  $\langle D \rangle \sim 0.9D$ , and with this fraction having a weak dependence on the refractive index.<sup>14</sup> Due to the exponential relationship between  $\Theta$  and  $\langle D \rangle$ , the most appropriate value of  $D$  to use in calculations for particles with a size distribution is typically not the average particle dimension, but is instead the minimum particle dimension or the minimum particle size if there is a distribution of particle sizes.<sup>14</sup> If the simple form of eq 7 is appropriate, then the absolute absorption coefficient can be calculated by combining eqs 3 and 7, giving the relationship:

$$\alpha = -\frac{1}{\langle D \rangle} \ln \left( \frac{w - S_e}{1 - S_e - S_i + S_i w} \right) \quad (8)$$

The absolute absorption spectrum of a loose powder can be directly calculated using from bidirectional reflectance data through this Hapke transform of eq 8. A flowchart of this process for obtaining  $\alpha(E)$  is provided in Figure 3. While knowledge of

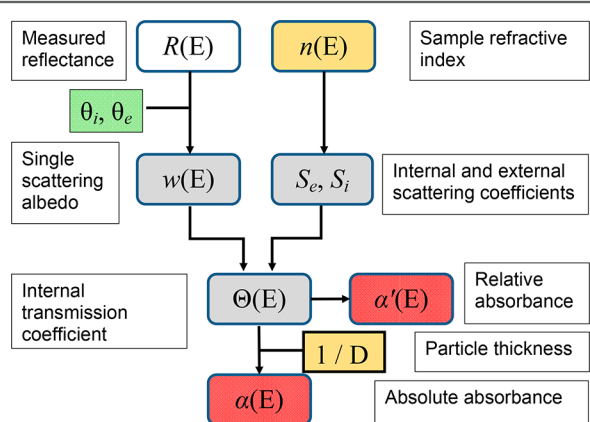


**Figure 3.** Flowchart of the process for calculating the absolute or relative absorbance of loose powder samples using a Hapke transform. White box indicates the primary input of optical data (reflectance), yellow boxes are other input data (obtained from measurements or theory), green box is reflectance measurement settings, gray boxes are derived parameters calculated from input data, and red boxes are physical properties that can be calculated. Knowledge of both the sample size and refractive index is needed for the calculation absorption coefficients,  $\alpha(E)$ , while only the refractive index is needed to calculate relative absorption coefficients,  $\alpha'(E)$ .

both  $n(E)$  and  $D$  is needed to calculate  $\alpha(E)$ ,  $\alpha'(E)$  does not require knowledge of the particle size. The absolute absorbance calculated this way has a simple inverse relationship with the particle size but a very complex relationship with the refractive index, which is described by eqs 1–8. Although the mathematical relationships are complex, they are indicative of a monotonic relationship between  $R(E)$  and  $\alpha(E)$  that can easily be computed (Figure S2).

Given the strongly nonlinear relationship between  $\alpha$  and  $\Theta$ , this formalism is only valid when the particle size distribution is relatively narrow. It should also be noted that eq 8 also assumes

that the loose powder sample is in a volume-scattering regime, where the reflectance of the sample is dominated by the refraction, transmission, and scattering of dense particles. This assumption is believed to be most effective when  $0.1 \lesssim \alpha D \lesssim 3$  (see ref 14). If other internal scattering processes are active within the particle, the simple form of eq 8 should be replaced by a more complex relationship that better describes the relationship between  $\alpha$  and  $\Theta$ , though such a treatment is beyond the scope of the present work.

#### Self-Referenced Determination of Refractive Index.

Among the three experimentally measured quantities ( $R$ ,  $n$ , and  $D$ ) needed to calculate  $\alpha(E)$  using the methods described in the previous section, the refractive index is the least experimentally accessible since there is no simple technique for the direct measurement of  $n$  for powder samples. Using integrating sphere (IS) reflectance data,  $\alpha'_{IS}(E)$  can be easily calculated without knowledge of  $n$  or  $k$  through a Kubelka–Munk transform:  $\alpha'_{IS} = (1 - R_{IS})^2 / (2R_{IS})$ . If the  $\alpha'_{IS}$  relative absorption data are used as a reference when analyzing bidirectional reflectance (BR) data,  $R_{BR}$ , then it is possible to treat  $n$  as a fit parameter and to then refine  $n$  so that the agreement between  $\alpha'_{IS}$  and  $\alpha'_{BR}$  is maximized. Sample size  $D$  does not influence the outcome, as it simply behaves as a linear adjustable scale factor.

This process for estimating  $n$  is demonstrated for the compounds  $\text{La}_4\text{Mo}_2\text{O}_{11}$ <sup>17</sup> and  $\text{La}_2\text{MoO}_5$ <sup>18</sup> in Figure 4. These compounds were chosen due to their complex optical spectrum due to the unusual direct metal–metal bonding present within these oxide compounds. In these initial fits, the energy dependence of  $n(E)$  was neglected since the variation of  $n$  is often only on the order of 10–20% across the spectral range of these measurements (0.5–3.5 eV). Other simple functional forms of  $n$  such as that of the Sellmeier equation<sup>19</sup> can be easily fit in a similar manner if modeling of the energy dependence of  $n$  is desired. In Figure 4,  $\alpha'_{IS}$  from integrating sphere data is shown in red and is compared to  $\alpha'_{BR}$  calculated for different values of  $n$ , shown as dashed black lines. Even within the constant  $n$  approximation, it is possible to obtain superb agreement between the relative absorption spectra inferred from integrating sphere and bidirectional reflectance data over the full range of energies studied. For both  $\text{La}_4\text{Mo}_2\text{O}_{11}$  and  $\text{La}_2\text{MoO}_5$ , the refined single value of  $n$  that best fit the data was 1.91. Larger or smaller values of  $n$  were unable to effectively reproduce the energy variation of  $\alpha'_{IS}$  over the measured energy range, with the most pronounced differences at energies above 1.5 eV. Although  $n$  has not

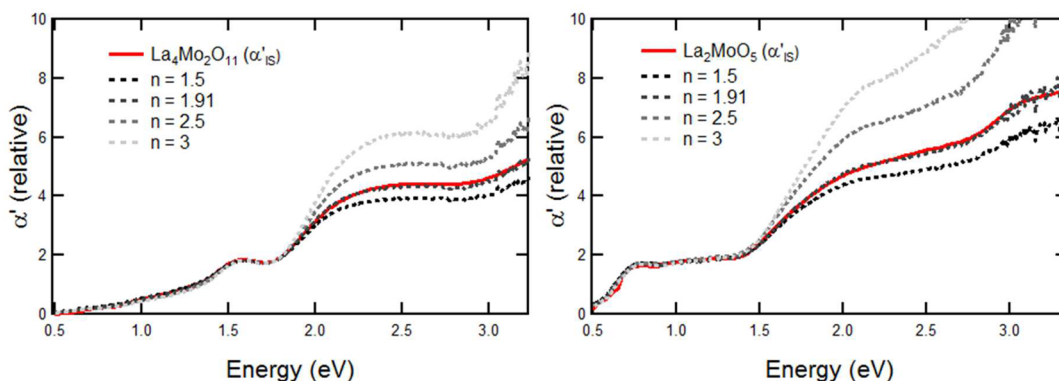


**Figure 4.** Comparison between relative absorption calculated from integrating sphere data,  $\alpha'_{IS}$  (red), and from bidirectional reflectance data,  $\alpha'_{BR}$  (dashed lines), when applying a Hapke transform for different constant values of  $n$  (black dashed lines) for the compounds  $\text{La}_4\text{Mo}_2\text{O}_{11}$  (left) and  $\text{La}_2\text{MoO}_5$  (right).

previously been measured for these complex semiconductors, the refined values of  $n$  fall between those measured over the energy range of 0.5–3.0 eV for the binary end members of  $\text{La}_2\text{O}_3$  (1.70–1.75)<sup>20</sup> and  $\text{MoO}_3$  (2.07–2.32).<sup>21</sup> This suggests that this novel self-referenced method is able to provide reasonable experimental estimates of the refractive indices of complex solids. It should be noted that the sensitivity to  $n$  is enhanced by carrying out the fitting over a large energy range, as the differences in fit quality at low energy data (0.5–1.5 eV) were small for a wide range of  $n$  values.

**Experimental Determination of Particle Diameter.** In addition to the refractive index, the representative particle diameter is also needed to calculate absolute absorbance from bidirectional reflectance data using a Hapke transform. To validate the use of a Hapke transform in calculating absolute absorbances, two classic semiconductors ( $\text{Fe}_2\text{O}_3$  and Ge) whose full optical coefficients ( $n$  and  $k$ ) have been previously determined in single crystal or thin film studies were chosen to serve as controls. Estimates of the particle size distribution were first made using the technique of laser diffraction, with measurements carried out on powders dispersed in sodium hexametaphosphate solutions and subjected to sonication treatments. The volume-weighted size distributions obtained in this manner are shown in Figure 5.

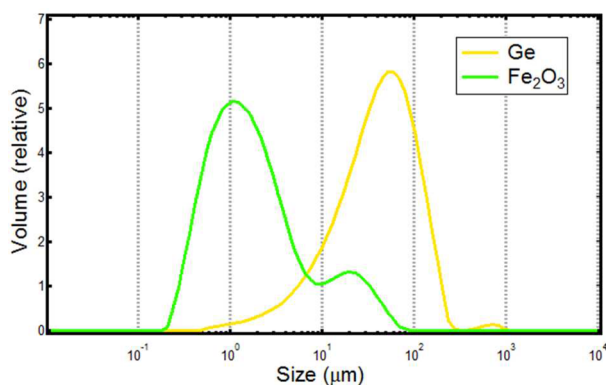


**Figure 5.** Particle size distribution from laser diffraction. The smaller  $\text{Fe}_2\text{O}_3$  peak at  $\sim 20 \mu\text{m}$  is attributed to agglomeration.

The laser diffraction experiments indicated a much smaller particle size for  $\text{Fe}_2\text{O}_3$  (mode of  $1 \mu\text{m}$ ) than for Ge (mode of  $50 \mu\text{m}$ ). A secondary peak maximum of  $20 \mu\text{m}$  was found for  $\text{Fe}_2\text{O}_3$ , which was tentatively attributed to the presence of a modest amount of larger aggregates due to imperfect dispersion of particles within the aqueous solution. Similarly, a small secondary peak at  $750 \mu\text{m}$  was also tentatively attributed to the aggregation of Ge particles. In both cases, it is expected that the aggregates are artifacts induced by the liquid-based measurement procedure and are not relevant to the analysis of reflectance data collected under dry conditions in which the attractive forces associated with the suspension of particles will be absent. The distribution of  $\text{Fe}_2\text{O}_3$  was much more symmetric than that of Ge, which exhibited a large tail extending to particle sizes 2 orders of magnitude smaller than the  $50 \mu\text{m}$  peak size. This distribution is particularly unfavorable for the determination of absolute optical properties since smaller particles have an exponentially larger influence on the measured reflectance than large particles.

Complementary direct measurements of particle size were obtained through SEM studies, with representative images shown in Figure 6. The Feret diameters for primary particles

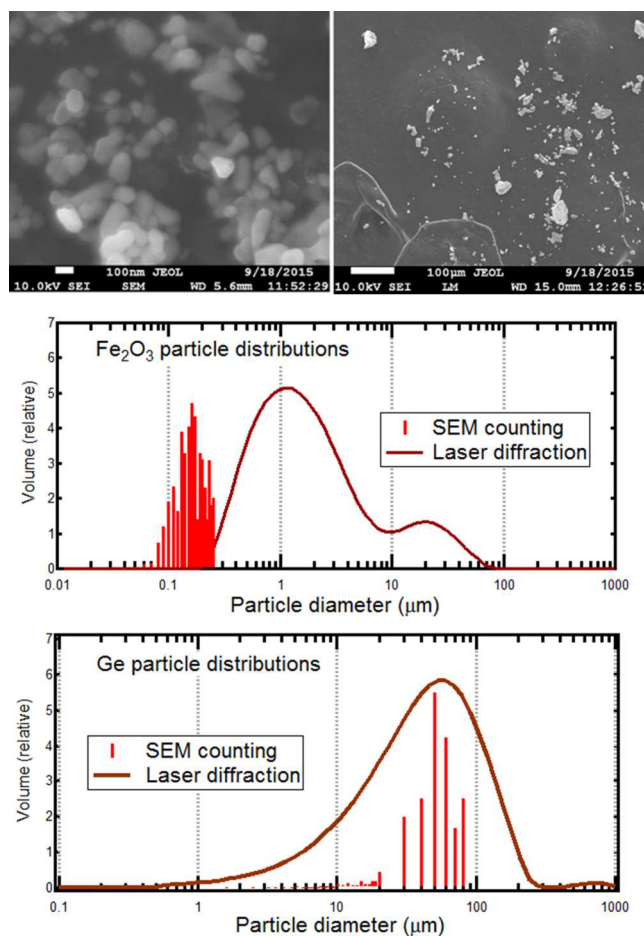


**Figure 6.** SEM images of  $\text{Fe}_2\text{O}_3$  (top left) and Ge (top right) together with the volume-weighted particle size distributions determined from the analysis of SEM images (red bars). The particle size distribution indirectly measured from laser diffraction (brown line) is overlaid for comparison. The total number of particles counted by SEM was about 150 for  $\text{Fe}_2\text{O}_3$  and 400 for Ge.

were automatically extracted using image analysis software.<sup>15,22</sup> No evidence was found in SEM images for the very large aggregates seen in the laser diffraction studies, suggesting that they indeed represent an aggregation phenomenon which only occurs in a liquid medium. It can be seen in SEM images that the primary particle size for  $\text{Fe}_2\text{O}_3$  is typically  $\sim 0.1 \mu\text{m}$ , though these primary particles are generally found in sintered clusters of secondary particles whose dimensions are consistent with the  $1 \mu\text{m}$  peak seen in laser diffraction studies. The distribution of Ge particles (wide variation in size with an extended tail to low particle sizes) inferred from laser diffraction measurements was confirmed by SEM studies. The lack of sintered aggregates in the Ge sample is consistent with this sample being prepared by milling from an initial preparation with a much larger particle size.

**Comparison to Single Crystal Data:  $\text{Fe}_2\text{O}_3$  Powders with a Narrow Size Distribution.** The absolute absorption coefficients of  $\text{Fe}_2\text{O}_3$  have been previously determined through transmission measurements on a single crystal sample.<sup>9</sup> These measurements can be used as a standard for evaluating the validity of calculations of absolute absorption from bidirectional reflectance data collected for loose powders using a Hapke transform. Rather than evaluating the absolute absorbance coefficients directly, the validity of loose powder methods was

tested by comparing the particle diameter predicted using different methods, as eq 8 shows that  $\alpha(E)$  is directly proportional to  $1/D$  at all energies.

Two different methods for obtaining the refractive index of  $\text{Fe}_2\text{O}_3$  for use in the Hapke transform were tested. First, a single-valued description of  $n = 2.3(1)$  was obtained using the self-referenced method for our powder sample (Figure S3). A reasonably close fit between  $\alpha'_{\text{IS}}$  and  $\alpha'_{\text{BR}}$  could be obtained in this manner, though there were small systematic deviations between the two calculated absorbances even with this best fit value of  $n$ . Second, data for  $n(E)$  previously measured for  $\text{Fe}_2\text{O}_3$  thin films<sup>23</sup> were parametrized using the formalism of the widely used Sellmeier equation:<sup>19</sup>

$$n^2 = A + \frac{B\lambda^2}{(\lambda^2 - C)} + \frac{D\lambda^2}{(\lambda^2 - E)} \quad (9)$$

Parameters  $D$  and  $E$  were neglected in fits as the inclusion of the last term typically has a very minor effect on the fit quality. The final fit (Figure 7) gave values of  $A = 4.485 \pm 0.063$ ,  $B = 2.397 \pm 0.053$ , and  $C = 0.208 \pm 0.002$ .

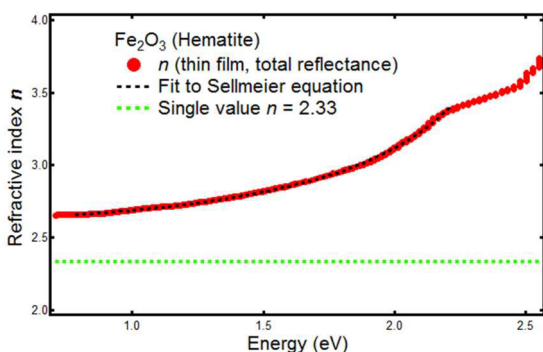


**Figure 7.** Experimentally measured hematite  $\text{Fe}_2\text{O}_3$  refractive index,  $n(E)$  (red solid line), and fit of these data (black dashed line) to three-parameter Sellmeier equation over the range of 0.8–2.2 eV with  $A$ ,  $B$ , and  $C$  coefficient values given in text. The single-valued result for  $n$  obtained from a one-parameter Sellmeier self-referenced fit ( $n = 2.3$ ) is shown (green dashed line) for comparison.

When evaluating the validity of the absolute absorbances obtained based on a self-referenced fit to  $n$  for loose powders or from Sellmeier fits to  $n(E)$  from crystalline films, the particle diameter was treated as a refined variable whose value was varied to maximize the quality of the fit between the literature  $\alpha(E)$  (black dashed line) obtained from single crystal transmission measurements and the Hapke  $\alpha(E)$  (solid colored lines) derived from loose powder measurements, as seen in Figure 8. The refined value of  $D$  was  $0.133 \mu\text{m}$  when using the thin film refractive index data and  $0.166 \mu\text{m}$  when using the self-referenced value of  $n = 2.3(1)$ . This indicates that the most appropriate particle size for the Hapke transform of this system is the primary particle size of  $0.16 \mu\text{m}$  determined from SEM and that using the larger secondary particle size of  $1 \mu\text{m}$  determined from laser diffraction experiments would result in the absolute absorption coefficients of this material being underestimated by about a factor of 10. The close agreement of the particle sizes estimated through the Hapke transform ( $0.133$ – $0.166 \mu\text{m}$ ) with the particle diameter measured in SEM studies ( $0.16 \mu\text{m}$ ) suggests that unknown absolute absorbances may be determined with errors of 25% or less under favorable conditions.

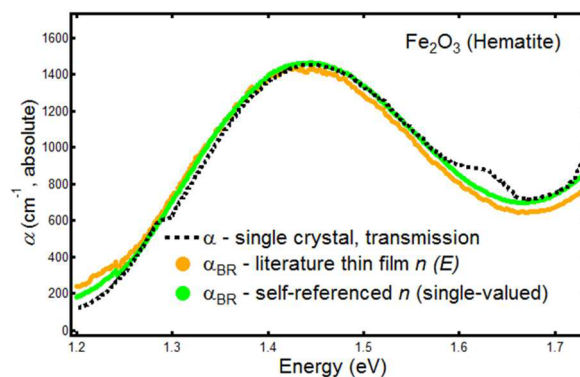


**Figure 8.** Comparison of the absolute absorption coefficients of  $\text{Fe}_2\text{O}_3$  obtained from single crystal transmission experiments<sup>9</sup> (dashed black line) with relative absorption spectra obtained from bidirectional reflectance data for loose powders using either a single value of  $n$  determined in a self-referenced manner (green solid line) or using  $n(E)$  previously determined from thin films<sup>23</sup> (solid orange line). The absolute absorbances obtained from loose powders will have exactly the same energy dependence but will differ in magnitude, as discussed in the main text.

As can be seen from this analysis, the greatest challenge in obtaining accurate absolute absorption coefficients from loose powder samples is obtaining powders with a nearly monodisperse size distribution and obtaining an accurate measurement of their size. Furthermore, it is advantageous to work with sample preparation methods that result in the production of isolated primary particles rather than leading to the formation of larger secondary particles. Preparation methods such as hydrothermal synthesis or the reductive milling of large primary particles are expected to be most effective in this regard.

Through the utilization of the Hapke formalism to describe the scattering of loose  $\text{Fe}_2\text{O}_3$  powders, the contribution of different terms influencing the overall reflectance of this sample can be separately plotted, as is done in Figure 9. As expected from eqs 1–5, the internal and external scattering coefficients primarily depend on  $n$  and do not substantially vary over the measurement range. The measured reflectance and the inferred single-scattering albedo behave in a similar manner as they both are related to the efficiency with which light is scattered from the

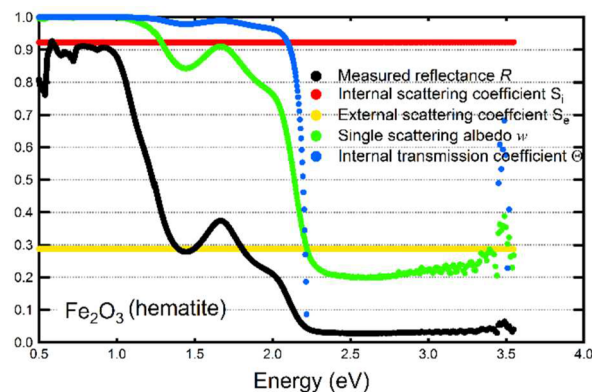


**Figure 9.** Energy variation of different parameters utilized in Hapke transforms for calculating the overall absorption coefficient of  $\text{Fe}_2\text{O}_3$  using  $n(E)$  previously determined from measurements on thin films, including the measured reflectance,  $R$ , as well as derived parameters such as the internal and external scattering coefficients,  $S_i$  and  $S_e$ ; the single-scattering albedo,  $w$ ; and the internal transmission coefficient,  $\Theta$ .

sample. Finally,  $\Theta$  describes the  $I/I_0$  ratio of light passing through the interior of  $\text{Fe}_2\text{O}_3$  particles and, as such, is directly related to their absorption coefficient. Good insights into  $\Theta$  cannot be obtained at energies beyond about 2.2 eV since at higher energies the sample powders nearly completely absorb incident light and for this reason provide very limited sensitivity to variations in  $\alpha$ .

**Comparison to Single Crystal Data: Ge Powders with a Wide Size Distribution.** The simple semiconductor Ge was used as a second reference compound used for evaluating the validity of calculations of absolute absorption from bidirectional reflectance data on loose powders. While the  $\text{Fe}_2\text{O}_3$  sample was in many ways ideally suited for this approach, the present Ge sample exemplifies many problems that can limit the validity of absorption coefficients calculated using a Hapke transform. The absorption spectrum of Ge near room temperature (300 K) is known to be characterized by an indirect gap with an energy of 0.62 eV and a direct gap with an energy of 0.81 eV.<sup>8</sup> In contrast to  $\text{Fe}_2\text{O}_3$ , which has weak absorption at the spectral regime over which single crystal transmission data were available, the direct Ge absorption is strong and saturates at energies just above the direct gap.

The refractive index of Ge was obtained both in a self-referenced manner with  $n = 1.93(3)$  (Figure S4) and also through the parametrization of existing literature data obtained from single crystals<sup>24,25</sup> using the autocollimation method.<sup>26</sup> When modeled using a three-parameter Sellmeier fit, the single crystal data yielded values of  $A = 8.996 \pm 0.211$ ,  $B = 7.150 \pm 0.169$ , and  $C = 0.340 \pm 0.057$ . The self-referenced and single crystal refractive index results are compared in Figure 10. It can

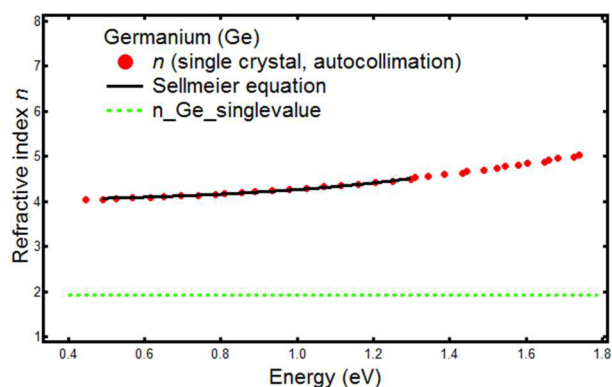


**Figure 10.** Experimentally measured Ge refractive index,  $n(E)$  (red solid line), and fit of these data (black dashed line) to a three-parameter Sellmeier equation over the energy range of 0.5–1.3 eV with  $A$ ,  $B$ , and  $C$  coefficient values given in the text.

be seen that the refined self-referenced value of  $n$  is about half of the literature value of  $n(E)$  obtained for single crystals. This huge discrepancy is attributed to the tremendously limited range of optical data on Ge suitable for analysis (0.7–0.8 eV), as can also be seen in the raw reflectance data (Figure S5). The narrow fitting range does not allow the refractive index to be effectively determined. This is consistent with the behavior seen for  $\text{La}_4\text{Mo}_2\text{O}_{11}$  and  $\text{La}_2\text{MoO}_5$  in Figure 4, where the energy dependence of the calculated absolute absorption was insensitive to the refractive index over the energy range of 0.5–1.5 eV but was very sensitive when calculated over the full energy range of 0.5–3.0.

The absolute absorption for Ge measured from single crystal transmission data can be compared to  $\alpha(E)$  from loose powders

(Figure 11), with the particle size again used as an adjustable parameter that reflects the quality of the absolute absorbance

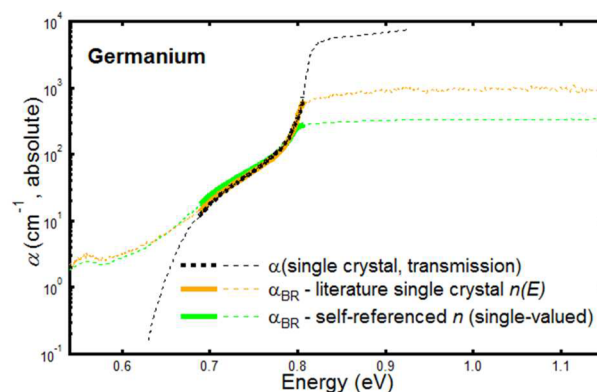


**Figure 11.** Comparison of the absolute absorption coefficients of  $\text{Fe}_2\text{O}_3$  obtained from single crystal transmission studies<sup>8</sup> (dashed black line) with the relative absorption spectra obtained from bidirectional reflectance data for loose powders using either a single value of  $n = 1.93$  determined in a self-referenced manner (green solid line) or using  $n(E)$  previously determined from single crystals<sup>26</sup> (solid orange line). Absolute absorbances obtained from loose powders have the same energy dependence as these relative absorbances, as discussed in the main text.

inferred from bidirectional reflectance data. The fit to the single crystal diffraction  $\alpha(E)$  is noticeably better using the refined single value of  $n$  instead of the more accurate experimentally determined  $n(E)$ . This is attributed to artifacts associated with trying to model the absorbance of particles with a wide size distribution using a mathematical model which assumes a single size of particle. From comparisons to the single crystal results, the effective particle size is calculated to be  $12.5 \mu\text{m}$  when using the self-referenced value of  $n = 1.93$ , and to be  $2.7 \mu\text{m}$  when using the literature values of  $n(E)$ . There is a large difference between these values due to the large difference in the magnitude of  $n$  used in the two Hapke transforms. Both inferred sizes are much smaller than the  $50 \mu\text{m}$  expected particle size based on laser diffraction and SEM measurements (Figure 6). It is generally expected that the smaller particle sizes will have a dominant effect on the calculated absolute absorbances, and this is indeed seen here. The extended low diameter tail in the Ge particle size distribution represents a worst case scenario for trying to accurately calculate absolute absorbances using the Hapke transform since the particle sizes with the largest effect on the measurement are present in small fractions that are difficult to model and quantify. It is expected that experimental efforts to narrow the size distribution of the semiconductor system (sieving, filtration, and sedimentation, etc.) could be used to narrow the size distribution and produce more reliable results, though such efforts are beyond the scope of the present work for this well-known semiconductor system.

The contribution of different terms in the Hapke transform influencing the calculated absorbance of Ge are separately plotted in Figure 12. The internal and external scattering coefficients determined for Ge do not substantially differ from those of  $\text{Fe}_2\text{O}_3$ , though the reflectance and single-scattering albedo are quite different, as expected given the very different nature of the light absorption for these two samples. The internal transmission coefficient is reduced to much smaller values over the spectral range of interest for Ge, consistent with the stronger

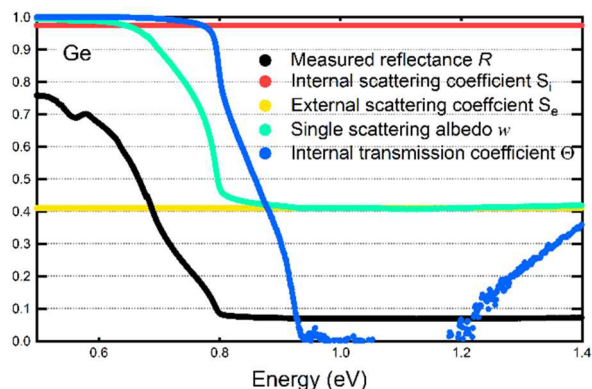


**Figure 12.** Energy variation of different parameters utilized in Hapke transforms for calculating the overall absorption coefficient of Ge using  $n(E)$  previously determined for a single crystal sample, including the measured  $R$  as well as derived parameters such as the internal and external scattering coefficients,  $S_i$  and  $S_e$ ; the single-scattering albedo,  $w$ ; and the internal transmission coefficient,  $\Theta$ .

absorption associated with the indirect and direct gaps of this compound relative to the forbidden  $d-d$  transition around 1.4 eV that was the primary feature in the energy range for  $\text{Fe}_2\text{O}_3$ . These plots are useful for identifying the energy ranges for which the Hapke transform approach is most likely to succeed, and conversely, also those regions in which the assumptions of this approach are most challenged.

## CONCLUSION

A method of determining the absolute absorption coefficients of loose powder samples through the application of a Hapke transform to bidirectional reflectance data has been demonstrated. In addition to the measured reflectance, information about the refractive index,  $n$ , and particle diameter is also needed to calculate absolute absorbances. If literature data for  $n$  are not available, it is shown that a novel self-referenced approach for determining  $n$  can be used in which the agreement is maximized between the relative absorption calculated from integrating sphere data (which is independent of  $n$ ) and bidirectional reflectance data (which depends on  $n$ ). Particle size data can be obtained from SEM (sensitive to primary particle size) or laser diffraction measurements (sensitive to secondary particle size), and the primary particle size was found to be most appropriate for correctly calculating the absolute absorption of  $\text{Fe}_2\text{O}_3$  powders. While these easy and rapid methods should be generally applicable to a wide variety of complex materials, it is demonstrated using Ge semiconductors that the self-referenced determination of  $n$  is not effective when the energy range of the measurable optical response is narrow and that the results obtained from the Hapke transform are not reliable when the particle size distribution is broad. To date, the absolute absorption coefficients of the majority of emerging semiconductors being studied for solar fuel production are completely unknown, and the present approach provides a means for rapidly obtaining first estimates of both the absolute absorption and refractive index of these materials.

## ASSOCIATED CONTENT

### Supporting Information

The Supporting Information is available free of charge on the ACS Publications website at DOI: 10.1021/acs.chemmater.6b04463.

Schematic of scattering processes, dependence of absolute absorbance on refractive index, self-referenced fits used to obtain single-valued  $n$ , bidirectional reflectance raw data. (PDF)

## AUTHOR INFORMATION

### Corresponding Author

\*E-mail: kpete@bnl.gov.

### ORCID

Peter G. Khalifah: 0000-0002-2216-0377

### Notes

The authors declare no competing financial interest.

Absorbance coefficients from bidirectional reflectance data were calculated using code written using the IgorPro graphing software, and code is available by request from the corresponding author.

## ACKNOWLEDGMENTS

This work was primarily supported by DOE Grant No. DE-FG02-11ER16266 with the U.S. Department of Energy. Studies on  $\text{La}_2\text{MoO}_5$  and  $\text{La}_4\text{Mo}_2\text{O}_{11}$  were supported by the National Science Foundation Grant No. DMR-0955646. Research carried out at Brookhaven National Laboratory was supported by the U.S. Department of Energy, Office of Basic Energy Sciences, under Contract No. DE-SC0012704. Research was carried out in part at the Center for Functional Nanomaterials, Brookhaven National Laboratory, which is supported by the U.S. Department of Energy, Office of Basic Energy Sciences, under Contract No. DE-SC0012704.

## REFERENCES

- (1) Kasahara, A.; Nukumizu, K.; Hitoki, G.; Takata, T.; Kondo, J. N.; Hara, M.; Kobayashi, H.; Domen, K. Photoreactions on  $\text{LaTiO}_2\text{N}$  under visible light irradiation. *J. Phys. Chem. A* **2002**, *106*, 6750–6753.
- (2) Yamasita, D.; Takata, T.; Hara, M.; Kondo, J. N.; Domen, K. Recent progress of visible-light-driven heterogeneous photocatalysts for overall water splitting. *Solid State Ionics* **2004**, *172*, 591–595.
- (3) Maeda, K.; Teramura, K.; Lu, D. L.; Takata, T.; Saito, N.; Inoue, Y.; Domen, K. Photocatalyst releasing hydrogen from water - Enhancing catalytic performance holds promise for hydrogen production by water splitting in sunlight. *Nature* **2006**, *440*, 295–295.
- (4) Chun, W. J.; Ishikawa, A.; Fujisawa, H.; Takata, T.; Kondo, J. N.; Hara, M.; Kawai, M.; Matsumoto, Y.; Domen, K. Conduction and valence band positions of  $\text{Ta}_2\text{O}_5$ ,  $\text{TaON}$ , and  $\text{Ta}_3\text{N}_5$  by UPS and electrochemical methods. *J. Phys. Chem. B* **2003**, *107*, 1798–1803.
- (5) Iizuka, K.; Wato, T.; Miseki, Y.; Saito, K.; Kudo, A. Photocatalytic Reduction of Carbon Dioxide over Ag Cocatalyst-Loaded  $\text{AlLa}_4\text{Ti}_4\text{O}_{15}$  ( $A = \text{Ca}, \text{Sr}, \text{and Ba}$ ) Using Water as a Reducing Reagent. *J. Am. Chem. Soc.* **2011**, *133*, 20863–20868.
- (6) Choi, T.; Lee, S.; Choi, Y. J.; Kiryukhin, V.; Cheong, S. W. Switchable Ferroelectric Diode and Photovoltaic Effect in  $\text{BiFeO}_3$ . *Science* **2009**, *324*, 63–66.
- (7) Schrebler, R. S.; Ballesteros, L.; Burgos, A.; Muñoz, E. C.; Grez, P.; Leinen, D.; Martín, F.; Ramos-Barrado, J. R.; Dalchiele, E. A. Electrodeposited nanostructured  $\alpha\text{-Fe}_2\text{O}_3$  photoanodes for solar water splitting: Effect of surface Co-modification on photoelectrochemical performance. *J. Electrochem. Soc.* **2011**, *158*, D500–D505.
- (8) Dash, W. C.; Newman, R. Intrinsic Optical Absorption in Single-Crystal Germanium and Silicon at 77 K and 300 K. *Phys. Rev.* **1955**, *99*, 1151–1155.
- (9) Marusak, L. A.; Messier, R.; White, W. B. Optical Absorption Spectrum of Hematite,  $\alpha\text{-Fe}_2\text{O}_3$  Near IR to UV. *J. Phys. Chem. Solids* **1980**, *41*, 981–984.
- (10) Grosse, P.; Offermann, V. Analysis of Reflectance Data Using the Kramers-Kronig Relations. *Appl. Phys. A: Solids Surf.* **1991**, *52*, 138–144.

(11) Yamamoto, K.; Masui, A.; Ishida, H. Kramers–Kronig Analysis of Infrared Reflection Spectra with Perpendicular Polarization. *Appl. Opt.* **1994**, *33*, 6285–6293.

(12) Salisbury, J. W.; Hapke, B.; Eastes, J. W. Usefulness of Weak Bands in Midinfrared Remote Sensing of Particulate Planetary Surfaces. *J. Geophys. Res.* **1987**, *92*, 702–710.

(13) Sklute, E. C.; Glotch, T. D.; Piatek, J. L.; Woerner, W. R.; Martone, A. A.; Kraner, M. L. Optical constants of synthetic potassium, sodium, and hydronium jarosite. *Am. Mineral.* **2015**, *100*, 1110–1122.

(14) Hapke, B. *Theory of Reflectance and Emittance Spectroscopy*, 2nd ed.; Cambridge University Press: New York, 2012; DOI: [10.1017/CBO9781139025683](https://doi.org/10.1017/CBO9781139025683).

(15) Schneider, C. A.; Rasband, W. S.; Eliceiri, K. W. NIH Image to ImageJ: 25 years of image analysis. *Nat. Methods* **2012**, *9*, 671–675.

(16) Kubelka, P.; Munk, F. Reflection characteristics of paints. *Z. Technol. Phys.* **1931**, *12*, 593–601.

(17) Gall, P.; Gougeon, P. Structure of  $\text{La}_4\text{Mo}_2\text{O}_{11}$  Containing Isolated  $\text{Mo}_2\text{O}_{10}$  Cluster Units. *Acta Crystallogr., Sect. C: Cryst. Struct. Commun.* **1992**, *48*, 1915–1917.

(18) Colabello, D. M.; Camino, F. E.; Huq, A.; Hybertsen, M.; Khalifah, P. G. Charge Disproportionation in Tetragonal  $\text{La}_2\text{MoO}_5$ , a Small Band Gap Semiconductor Influenced by Direct Mo–Mo Bonding. *J. Am. Chem. Soc.* **2015**, *137*, 1245–1257.

(19) Ghosh, G. *Handbook of Thermo-Optic Coefficients of Optical Materials with Applications*; Academic Press: New York, 1998.

(20) Atuchin, V. V.; Kalinkin, A. V.; Kochubey, V. A.; Kruchinin, V. N.; Vemuri, R. S.; Ramana, C. V. Spectroscopic ellipsometry and x-ray photoelectron spectroscopy of  $\text{La}_2\text{O}_3$  thin films deposited by reactive magnetron sputtering. *J. Vac. Sci. Technol., A* **2011**, *29*, 021004.

(21) Lajaunie, L.; Boucher, F.; Dessapt, R.; Moreau, P. Strong anisotropic influence of local-field effects on the dielectric response of  $\alpha\text{-MoO}_3$ . *Phys. Rev. B: Condens. Matter Mater. Phys.* **2013**, *88*, 115141.

(22) Merkus, H. G. *Particle Size Measurements: Fundamentals, Practice, Quality*; Springer: 2009.

(23) Glasscock, J. A.; Barnes, P. R. F.; Plumb, I. C.; Bendavid, A.; Martin, P. J. Structural, optical and electrical properties of undoped polycrystalline hematite thin films produced using filtered arc deposition. *Thin Solid Films* **2008**, *516*, 1716–1724.

(24) Salzberg, C. D.; Villa, J. J. Infrared Refractive Indexes of Silicon Germanium and Modified Selenium Glass. *J. Opt. Soc. Am.* **1957**, *47*, 244–246.

(25) Philipp, H. R.; Taft, E. A. Optical Constants of Germanium in the Region 1 to 10 eV. *Phys. Rev.* **1959**, *113*, 1002–1005.

(26) McAlister, E. D.; Villa, J. J.; Salzberg, C. D. Rapid and Accurate Measurements of Refractive Index in the Infrared. *J. Opt. Soc. Am.* **1956**, *46*, 485–487.

#### ■ NOTE ADDED AFTER ASAP PUBLICATION

This paper was published on May 22, 2017, with an error in Figure 3. The corrected version was reposted on May 24, 2017.